A STUDY OF THE SINGULARITY IN THE DIE-SWELL PROBLEM

By W. W. SCHULTZ

(*Department of Mechanical Engineering and Applied Mechanics, University of Michigan, Ann Arbor, Michigan* 48109, *USA*)

and C. GERVASIO

(*Department of Mechanical and Aerospace Engineering, Rutgers University, Piscataway, New Jersey* 08854, *USA*)

[Received 17 August 1989]

SUMMARY

The matched-eigenfunction method of Trogdon and Joseph is improved and used to solve the die-swell problem in an axisymmetric Newtonian liquid jet. The improved solution is the first computation that is consistent with the local analysis of Michael at the separation point. The stream function is expanded using two sets of eigenfunctions to describe the flow inside and outside the die, and these are matched at the exit to determine the expansion coefficients. The discontinuity in the shear-stress boundary condition at the jet exit causes spurious solution oscillations that are reduced significantly using the adjoint method used here. The orthogonal properties of the method reduce the algebraic system by one-half, and the complex-conjugate property of the coefficients reduces the system by one-half again. The reductions in oscillations and size of the system are important because the local behaviour at the contact line can only be obtained by extrapolation of the computations to high truncation.

1. Introduction

THE die-swell problem (see Fig. 1) is an important computational test for Newtonian (**1**, **2**) and viscoelastic (**3**, **4**) flows with free surfaces. During the transition from the fully-developed flow upstream to the plug-flow downstream, the jet swells due to stress relaxation at the outer surface. Die swell is usually associated with the low-Reynolds-number flow of viscoelastic fluids, but it occurs to a lesser extent in Newtonian fluids as well. Here we consider only Stokes flow of a Newtonian fluid.

The results of these computations (**1** to **4**) agree well with experiments (**5**, **6**) in describing the global structure of the flow. For example, all predict approximately a 13 per cent die swell (that is, the final jet radius is approximately 1·13 times the die radius) in a Newtonian jet with zero surface tension and small Reynolds number. However, they all fail to model the singularity at the die exit (or contact line where the solid, liquid, and gas meet, as represented by $\bar{r} = 0$ in Fig. 2). Consequently, they all show separation at other than 180 degrees, which violates a local condition described by Michael (**7**).

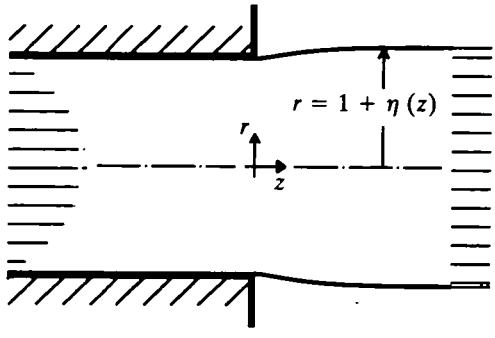

FIG. 1. Schematic of die swell in an axisymmetric jet

Our goal is to develop an improved computational technique so that we can improve the missing local mechanics of previous computations at the contact line. A careful examination of the flow in the neighbourhood of the singularity is required for several reasons. First, the flow in this region will determine whether the contact line will move on to the die outer face. This 'wetting' ($\alpha = 270°$ in Fig. 2) is undesirable in manufacturing processes. A second reason is that it is believed (**4, 8**) that the computational difficulties of highly viscoelastic flows are caused by the flow singularity. Understanding the singular behaviour in Newtonian flow may guide these viscoelastic computations.

There have been some attempts to model separation in die swell. Silliman and Scriven (**9**) add slip to their model as a way of relaxing the effect of the singularity at the contact line but otherwise do not capture the true singular behaviour as the slip parameter goes to zero. Most computations use mesh refinement near the singularity, but a careful examination of these finite-element computations shows that refinement is often insufficient because oscillations occur at the singularity (**10**). Sturges (**11**) states, but does not explain (presumably due to the singular nature of separation), that the free surface can separate at angles other than 180° if free-surface curvature is considered. (The effect of surface tension and infinite curvature has been examined previously for potential flow (**12**).) A boundary-integral method is used to study separation by Tanner *et al.* (**13**). They find that the local

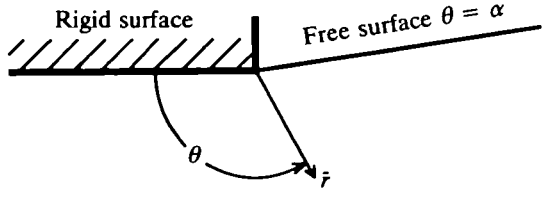

FIG. 2. Schematic of local separation of free surface

condition defined by Michael does not appear to be violated in the limit as the rounding of the die exit becomes very large. However, their computations lead to the same inconsistency when the die exit is sharp.

We modify the matched-eigenfunction method developed by Trogdon and Joseph (**14, 15**) to study the separation phenomena as affected by the singularity. Like the other methods mentioned above, this one makes no special provisions for the singularity; hence, we must interpret the results carefully. The development of this technique started with the 'stick–slip' problem by Richardson (**16**), in which boundary conditions are imposed that prohibit the jet from swelling or contracting. Richardson solves this problem by a Fourier transform in the axial direction and then applies the Wiener–Hopf technique to ensure continuation between the regions inside and outside the die. He states that a perturbation of the stick–slip solution can model die swell with large surface tension by using the capillary number as a small parameter, but recognizes that the results so obtained contradict the local solution of Michael (**7**).

Trogdon and Joseph (**14**) compare the Wiener–Hopf method used by Richardson with a matched-eigenfunction expansion method for the infinite-surface-tension stick–slip problem in a round jet. They find that for a given truncation of the infinite series, the matched-eigenfunction expansion gives better results than the Wiener–Hopf method, even though the latter gives the exact coefficients for infinite truncation. Their method also eliminates the slowly-converging infinite products of the Wiener–Hopf method. Trogdon and Joseph (**15**) then consider the die-swell problem with finite surface tension using the matched-eigenfunction method. This requires linearizing the free-surface boundary conditions about $r = 1$. Sturges (**17**) examines a planar jet using the same method considering second-order as well as Newtonian fluids.

We first re-examine the local analysis of Michael (**7**) in the vicinity of the singularity at the contact line of the jet exit in section 2. After posing the global problem, an improved eigenfunction-expansion method for the linearized die-swell problem is developed, expanding the work of (**15**) in section 3. In section 4 we show that our method of taking inner products with the adjoint eigenvectors reduces the oscillations as compared to computations where non-orthogonal functions are used in the inner products. We review our findings in section 5 and indicate the weaknesses of the improved matched-eigenfunction method by demonstrating that the free-surface linearization is not appropriate for many cases. Methods for further study are proposed.

2. Local analysis at separation

A local solution to the Stokes equation is a superposition of (**18, 7**)

$$\tilde{\psi} = \tilde{r}^{\lambda}[A \sin \lambda\theta + B \cos \lambda\theta + C \sin (\lambda - 2)\theta + D \cos (\lambda - 2)\theta], \qquad (1)$$

with other forms for special cases not considered here. Here, $\tilde{\psi}$ is the standard two-dimensional stream function and $\tilde{r}$ and θ are shown in Fig. 2.

The eigenequation

$$\sin(\lambda-1)\alpha \pm (\lambda-1)\sin\alpha = 0 \tag{2}$$

determines permissible values of λ. As is true of all local solutions, the solution contains one undetermined constant that must be obtained from a global solution. The local solutions result in radial and circumferential velocities proportional to $\tilde{r}^{\lambda-1}$ and pressure and stresses proportional to $\tilde{r}^{\lambda-2}$. To avoid infinite velocities we restrict to $\lambda > 1$.

When $\theta = \alpha = \pi$, the infinite pressures and viscous terms cancel each other and the values of λ are given by

$$\lambda = \tfrac{3}{2}, 2, \tfrac{5}{2}, 3, \ldots . \tag{3}$$

Hence, in the absence of surface tension, Michael (7) concludes that the free surface must separate at an angle $\alpha = \pi$. This conclusion contradicts experimental and computational observations that show the free surface separating at angles other than 180°.

The free surface can be considered flat in the vicinity of the contact line if (a) we examine a region much smaller than the die radius r_i to neglect azimuthal curvature, and (b) the curvature in the axial direction is at most weakly singular. Consider a free-surface shape given by

$$\eta = f(z) = \begin{cases} 0, & z < 0, \\ bz + cz^n, & z > 0 \end{cases} \tag{4}$$

as $z \to 0$. Neglecting the azimuthal component, the curvature is given by $f''/(1+f'^2)^{\frac{3}{2}}$, so the surface (4) has infinite curvature as $z \to 0$ if $\frac{1}{2} < n < 2$. Limiting the curves to finite slope (so the fluid does not wet the outer face of the die as when $\alpha = 270°$) further restricts n such that $1 < n < 2$, so the corner angle is determined only by b.

Even though the free-surface curvature is infinite under these conditions, the local analysis of Michael still applies. Then, if the surface-tension coefficient is non-zero, the surface can separate at an angle other than 180°, because the surface curvature (4) has the same singular form as the normal stress predicted by Michael. Specifically, if the angle of separation α is close to π, then $b \to 0$ in (4), and z of (4) is equivalent to $\tilde{r}$ in (1). The stresses will have the form $\tilde{r}^{\lambda-2}$, with the smallest λ close to the $\frac{3}{2}$ given by (3). The infinite normal stress can be balanced by surface tension if $n = \lambda$. Hence for small surface tension, we may expect a free surface of form (4) with small b and $n = \lambda \approx \frac{3}{2}$.

If the separation angle is known, then the nature of the singularity is known; that is, $n = n(b)$. Unfortunately, because the problem is elliptic, b and c must be determined from the global solution. We shall show that this is consistent with our global computed solutions. When surface tension is

non-zero, the separation angle is variable and the curvature becomes infinite. When the surface tension is zero, the free surface separates at 180 degrees although macroscopically that may not appear to be the case.

If slip is added at the solid wall, the local eigenfunction solution no longer exists. This indicates that the singularity has been relieved and the Michael separation condition no longer applies. However, we would again expect the free surface to separate at 180 degrees because the derivative of a streamline direction cannot be discontinuous in a region of non-zero velocity without requiring unbounded viscous and inertial forces.

3. Problem formulation

Consider a steady axisymmetric liquid jet with constant properties exiting from a constant-diameter die (Fig. 1) into an inviscid gas with pressure set to zero. The effect of gravity is neglected. The axial velocity is assumed to be parabolic far upstream, and it becomes independent of the radial and axial directions ('plug' or rectilinear flow) far downstream. The die radius is r_i, and the velocity in the radial and axial directions is u and w, respectively. We further assume that v (the swirl velocity) is zero. To non-dimensionalize the equations, velocities are scaled by the average axial velocity at the die w_i. Lengths are scaled by the die radius r_i, time is scaled by r_i/w_i, and the pressure scale is $\mu w_i/r_i$. The equation of motion then becomes

$$\mathscr{L}^2\psi = 0, \qquad \text{where } \mathscr{L} \equiv r\frac{\partial}{\partial r}\left(\frac{1}{r}\frac{\partial}{\partial r}\right) + \frac{\partial^2}{\partial z^2}, \tag{5}$$

ψ is the axisymmetric stream function such that

$$u = -\frac{1}{r}\psi_z, \qquad w = \frac{1}{r}\psi_r, \tag{6}$$

and r and z subscripts denote radial and axial derivatives, respectively. No-slip boundary conditions are usually applied inside the die, $z<0$, although we also consider a slip coefficient as in (**9**). On the free surface, defined by $r = R(z)$, $z>0$, the normal stress is balanced by the surface-tension coefficient times curvature:

$$p - \frac{2}{1+R'^2}[u_r + R'^2 w_z - R'(u_z + w_r)] = \mathrm{Ca}^{-1}\left[\frac{1+R'^2 - RR''}{R(1+R'^2)^{\frac{1}{2}}}\right], \tag{7}$$

where the capillary number is defined by $\mathrm{Ca} = \mu w_i/\sigma$, and σ is the surface-tension coefficient. The inviscid environment imposes no shear stress on the free surface:

$$2R'(u_r - w_z) + (1 - R'^2)(u_z + w_r) = 0. \tag{8}$$

Finally, the free-surface kinematic boundary condition requires that

$$\frac{D[r - R(z)]}{Dt} = u - wR' = 0. \tag{9}$$

In addition, all physical quantities such as velocities and stresses are finite at $r = 0$. In the case of infinite surface tension (zero capillary number), the pressure difference across the free surface is infinite and we have one less unknown since the free surface is cylindrically shaped.

Linearized, free-surface boundary conditions

The free surface swells by 13 per cent in typical finite-element calculations without surface tension; less when surface tension is present. Because the jet swell is small, we expand the free-surface boundary conditions (7) to (9) about a cylinder of $r = 1$. Following Trogdon and Joseph (**15**), we separate components of the pressure and the stream function from their asymptotic values as $z \to \infty$:

$$\psi(z, r) = \tfrac{1}{2} U_f r^2 + \tilde{\psi}(z, r) \tag{10}$$

and

$$p(z, r) = \frac{\mathrm{Ca}^{-1}}{1 + \eta_f} + \tilde{p}(z, r), \tag{11}$$

where U_f is the rectilinear flow velocity. Describing the free-surface location by $R(z) = 1 + \eta(z)$, we then assume that η, $\tilde{\psi}$, and $\tilde{p}$ and all their z-derivatives are small, and discard the nonlinear quantities to obtain

$$-\left(\frac{2}{r}\tilde{\psi}_z\right)_r - \tilde{p} + \mathrm{Ca}^{-1}\eta_f - \mathrm{Ca}^{-1}(\eta'' + \eta) = 0, \tag{12}$$

$$-\frac{1}{r}\tilde{\psi}_{zz} + \left(\frac{1}{r}\tilde{\psi}_r\right)_r = 0 \tag{13}$$

and

$$-\frac{1}{r}\tilde{\psi}_z - \eta' U_f = 0. \tag{14}$$

Since the boundary conditions have been transferred to a constant coordinate $r = 1$, we may take a z-derivative of (12) to eliminate the constant term and to substitute the pressure gradient from the z-momentum equation. Equation (14) is then used to eliminate the η'- and η'''-terms. Integrating (14) and using the boundary condition $\psi(1, 0) = 1$ gives

$$\eta(z) = \frac{1}{U_f}[1 - \tfrac{1}{2}U_f - \tilde{\psi}(z, 1)]. \tag{15}$$

The flow is represented using separate eigenfunctions inside and outside the die that are matched at the exit, $z = 0$. The stream functions inside and

outside the die are given respectively by

$$\psi(z, r) = \frac{2r^2 - r^4 + 4\beta r^2}{1 + 4\beta} + \sum_{n=-\infty}^{\infty} \frac{C_n}{p_n^2} \phi_n(r) \exp(p_n z), \qquad z < 0, \tag{16}$$

$$\hat{\psi}(z, r) = \tfrac{1}{2} U_f r^2 + \sum_{n=-\infty}^{\infty} \frac{D_n}{\alpha_n^2} \hat{\phi}_n(r) \exp(-\alpha_n z), \qquad z > 0. \tag{17}$$

As $z \to \pm\infty$, the flow reduces to the Poiseuille (with slip) and rectilinear flows, respectively. For the sake of completeness, we have introduced a dimensionless Navier slip coefficient β, such that $w + \beta w_r = 0$ on the solid surface at $r = 1$. The no-slip limit is recovered in the limit $\beta \to 0$. In this case, the far-field solution becomes Poiseuille flow $\psi = r^2(2 - r^2)$. Substituting (16) and (17) into (5) leads to two eigenvalue problems: inside the die,

$$(L + p_n^2)^2 \phi_n = 0, \tag{18}$$

with the solid-wall boundary conditions $\phi_n(1) = \beta\phi_n''(1) + \phi_n'(1) = 0$; in the jet,

$$(L + \alpha_n^2)^2 \hat{\phi}_n = 0, \tag{19}$$

with linearized boundary conditions applied at $r = 1$ that are given by

$$\hat{\phi}_n'' - \hat{\phi}_n' - \alpha_n^2 \hat{\phi}_n = 0 \tag{20}$$

and

$$\hat{\phi}_n''' - 2\hat{\phi}_n'' + (2 + 3\alpha_n^2)\hat{\phi}_n' - (2\alpha_n^2 - \mathrm{Ca}^{-1}\alpha_n^3 - \mathrm{Ca}^{-1}\alpha_n)\hat{\phi}_n = 0. \tag{21}$$

Here, L is a second-order ordinary differential operator given by the first term of $\mathscr{L}$. The eigenfunctions are (**15**)

$$\phi_n = J_0(p_n) r J_1(p_n r) - J_1(p_n) r^2 J_0(p_n r) \tag{22}$$

and

$$\hat{\phi}_n = [J_1(\alpha_n) + \alpha_n J_0(\alpha_n)] r J_1(\alpha_n r) - \alpha_n J_1(\alpha_n) r^2 J_0(\alpha_n r). \tag{23}$$

The eigenvalues are found numerically using a complex-valued secant method from the characteristic equations:

$$p_n J_0^2(p_n) - 2J_0(p_n)J_1(p_n) + (1 + 2\beta) p_n J_1^2(p_n) = 0 \tag{24}$$

and

$$\alpha_n^2 J_0^2(\alpha_n) + \left[(\alpha_n^2 - 1) + \left(\frac{\alpha_n^2 + 1}{2\alpha_n}\right) \frac{1}{\mathrm{Ca}\, U_f}\right] J_1^2(\alpha_n) = 0. \tag{25}$$

In the limit of infinite surface tension, the eigenvalues of (25) reduce to the roots of $J_1(\alpha_n) = 0$, which are used for the Galerkin inner products in (**15**). In the limit as $n \to \infty$, the eigenvalues differ by $(\pi, 0)$, making it easy to

TABLE 1. *Outside eigenvalues* α_n

n	$(\mathrm{Ca}\ U_f)^{-1}=0$	$(\mathrm{Ca}\ U_f)^{-1}=1$	$(\mathrm{Ca}\ U_f)^{-1}=10$	$(\mathrm{Ca}\ U_f)^{-1}=100$
1	(2·8105, 1·3399)	(3·1091, 1·3046)	(3·6671, 0·7515)	(3·8122, 0·2641)
2	(6·0947, 1·6342)	(6·3478, 1·6052)	(6·8631, 0·9848)	(6·9964, 0·3624)
3	(9·2888, 1·8265)	(9·5318, 1·7914)	(10·0291, 1·1369)	(10·1546, 0·4347)
4	(12·4587, 1·9661)	(12·6977, 1·9268)	(13·1850, 1·2518)	(13·3051, 0·4940)
5	(15·6183, 2·0755)	(15·8552, 2·0333)	(16·3362, 1·3446)	(16·4523, 0·5451)
10	(31·3655, 2·4185)	(31·5992, 2·3700)	(32·0671, 1·6498)	(32·1725, 0·7340)
20	(62·8039, 2·7639)	(63·0364, 2·7118)	(63·4977, 1·9734)	(63·5956, 0·9687)
30	(94·2280, 2·9663)	(94·4603, 2·9131)	(94·9194, 2·1681)	(95·0144, 1·1253)

verify that the expansion functions are complete. The forms (16) and (17) require eigenvalues with positive real parts. Selected eigenvalues from (24) and (25) are listed in Tables 1 and 2, respectively. The eigenvalues come in conjugate pairs, so only those with positive imaginary parts are listed.

We find it advantageous to express equations (18) and (19) in the standard form for an eigenvalue problem in order to find the adjoint eigenvalue system. In a manner similar to but not the same as Smith (**19**) and extended to axisymmetric Stokes flow by Yoo and Joseph (**20**), we obtain the standard form as

$$\mathbf{M}\begin{pmatrix}\phi_n\\ \gamma_n\end{pmatrix}=-p_n^2\begin{pmatrix}\phi_n\\ \gamma_n\end{pmatrix} \tag{26}$$

and

$$\mathbf{M}\begin{pmatrix}\hat{\phi}_n\\ \hat{\gamma}_n\end{pmatrix}=\alpha_n^2\begin{pmatrix}\hat{\phi}_n\\ \hat{\gamma}_n\end{pmatrix}, \tag{27}$$

where

$$\mathbf{M}=\begin{bmatrix}L & -1\\ 0 & L\end{bmatrix} \tag{28}$$

and L is the previously defined second-order ordinary differential operator. The auxiliary functions γ_n and $\hat{\gamma}_n$ are formed for convenience but are related to the vorticity in the same way that ϕ_n and $\hat{\phi}_n$ are related to the stream

TABLE 2. *Inside eigenvalues* p_n

n	$\beta=0$	$\beta=0{\cdot}01$	$\beta=0{\cdot}1$
1	(4·46629, 1·46747)	(4·42362, 1·45145)	(4·18224, 1·27376)
2	(7·69410, 1·72697)	(7·62127, 1·70499)	(7·28320, 1·41216)
3	(10·87457, 1·89494)	(10·77266, 1·86626)	(10·38285, 1·46876)
4	(14·03889, 2·02006)	(13·90878, 1·98357)	(13·49336, 1·49633)
5	(17·19556, 2·11994)	(17·03820, 2·07449)	(16·61235, 1·51146)
10	(32·93833, 2·44213)	(32·66063, 2·33772)	(32·26587, 1·53519)
20	(64·37527, 2·77608)	(63·93553, 2·52568)	(63·65046, 1·54205)
30	(95·79914, 2·97457)	(95·26786, 2·58786)	(95·05548, 1·54339)

function; that is,

$$\begin{pmatrix}\psi\\ r\omega\end{pmatrix}=\frac{1}{1+4\beta}\begin{pmatrix}2r^2-r^4+4\beta r^2\\ -8r^2\end{pmatrix}+\sum_{-\infty}^{\infty}\frac{C_n}{p_n^2}\begin{pmatrix}\phi_n(r)\\ \gamma_n(r)\end{pmatrix}e^{p_n z}, \tag{29}$$

$$\begin{pmatrix}\hat{\psi}\\ r\hat{\omega}\end{pmatrix}=\begin{pmatrix}\frac{1}{2}U_f r^2\\ 0\end{pmatrix}+\sum_{-\infty}^{\infty}\frac{D_n}{\alpha_n^2}\begin{pmatrix}\hat{\phi}_n(r)\\ \hat{\gamma}_n(r)\end{pmatrix}e^{-\alpha_n z}. \tag{30}$$

Adjoint eigenvalue problem

For matching, we need only develop the adjoint system for either the inside or outside of the die. We develop the adjoint system for the inside, since the boundary conditions are simpler. The natural definition for the inner product of the solution vector is

$$\langle \mathbf{x}, \mathbf{y}\rangle = \int_0^1 \frac{1}{r}\mathbf{x}\cdot\mathbf{y}^*\,dr. \tag{31}$$

Here, * denotes the complex conjugate and $\mathbf{x}$ and $\mathbf{y}$ are vector functions of r. From (31), the adjoint operator is the transpose, $\tilde{\mathbf{M}}=\mathbf{M}^T$, resulting in the adjoint eigenfunction $\tilde{\mathbf{x}}_n=[\gamma_n^*, \phi_n^*]^T$. It is the complex conjugate of the original eigenvector but 'upside down'. In addition to showing that the eigenvalues and adjoint eigenvalues are identical, it is easily shown that the adjoint eigenfunctions are orthogonal to the eigenfunctions of the inside expansion (**21**); that is,

$$\left\langle\begin{pmatrix}\phi_n(r)\\ \gamma_n(r)\end{pmatrix}, \begin{pmatrix}\gamma_m^*(r)\\ \phi_m^*(r)\end{pmatrix}\right\rangle = 0 \quad \text{if } n\neq m. \tag{32}$$

Matching

By matching, we can find the sets of complex coefficients C_n and D_n for continuous solutions at the die exit. The coefficients will vary depending on which of many methods is chosen. Trogdon and Joseph (**14**, **15**) match the stream function and the first three z-derivatives at $z=0$. This is sufficient to ensure a continuous solution at the matching location for the fourth-order operator. However, we match the stream function and r times vorticity, and their first z-derivatives:

$$\begin{pmatrix}\hat{\psi}\\ r\hat{\omega}\end{pmatrix}(r, 0^+)=\begin{pmatrix}\psi\\ r\omega\end{pmatrix}(r, 0^-) \tag{33}$$

and

$$\begin{pmatrix}\hat{\psi}_z\\ r\hat{\omega}_z\end{pmatrix}(r, 0^+)=\begin{pmatrix}\psi_z\\ r\omega_z\end{pmatrix}(r, 0^-), \tag{34}$$

where ω is the only non-zero component of vorticity, and is given by $\omega = w_r - u_z = (1/r)\mathcal{L}\psi$. Taking inner products of (34) with the conjugate

of the inside adjoint eigenfunctions $\tilde{\mathbf{x}}_n$, and truncating the infinite sum to N, yields

$$\sum_{-N}^{N} \frac{D_n}{\alpha_n^2}(A_{mn} - G_{mn}) = f_m + \frac{C_m}{p_m^2} B_m \tag{35}$$

and

$$\sum_{-N}^{N} \frac{D_n}{\alpha_n} A_{mn} = -\frac{C_m}{p_m} B_m, \tag{36}$$

where U_f has been eliminated using (30) evaluated at $r = 1$ and $z = 0$. The orthogonality property allows C_m to be eliminated from these equations to reduce the linear system by half, giving

$$\sum_{-N}^{N} \frac{D_n}{\alpha_n^2}\left(A_{mn} - G_{mn} + \frac{\alpha_n}{p_m} A_{mn}\right) = f_m. \tag{37}$$

The coefficients are

$$A_{mn} = \left\langle \begin{pmatrix} \phi_n(r) \\ \gamma_n(r) \end{pmatrix}, \begin{pmatrix} \gamma_m(r) \\ \phi_m(r) \end{pmatrix} \right\rangle = \frac{2p_m J_1(p_m)}{(\alpha_n^2 - p_m^2)} [\alpha_n J_0(\alpha_n) J_1(\alpha_n) J_1(p_m)$$

$$- \alpha_n^2 J_0^2(\alpha_n) J_1(p_m) + p_m J_1^2(\alpha_n) J_0(p_m) - \alpha_n^2 J_1^2(\alpha_n) J_1(p_m)] + F(\beta, m, n), \tag{38}$$

$$G_{mn} = \left\langle \begin{pmatrix} r^2 \hat{\phi}_n(1) \\ 0 \end{pmatrix}, \begin{pmatrix} \gamma_m(r) \\ \phi_m(r) \end{pmatrix} \right\rangle = 2J_1^2(\alpha_n) J_1(p_m)\left[2\frac{J_1(p_m)}{p_m} - J_0(p_m)\right], \tag{39}$$

$$f_m = \left\langle \begin{pmatrix} r^2(1-r^2) \\ -8r^2 \end{pmatrix}, \begin{pmatrix} \gamma_m(r) \\ \phi_m(r) \end{pmatrix} \right\rangle = \frac{-4J_1^2(p_m)}{p_m}, \tag{40}$$

and

$$B_m = \left\langle \begin{pmatrix} \phi_m(r) \\ \gamma_m(r) \end{pmatrix}, \begin{pmatrix} \gamma_m(r) \\ \phi_m(r) \end{pmatrix} \right\rangle = -2J_1^4(p_m) - 4p_m \beta J_0(p_m) J_1^3(p_m), \tag{41}$$

where $F(\beta, m, n)$ is a complicated function that becomes zero for the no-slip case $\beta \to 0$. We do not list $F(\beta, m, n)$ here. These integrations were performed with the symbolic manipulator REDUCE and with the aid of some integrals listed by Yoo and Joseph (**20**). The integrals were checked by numerical integration.

Because D_n and D_{-n} are complex conjugates, we need solve for only $2N$ real unknowns, $\Re(D_n)$ and $\Im(D_n)$ for $n = 1, 2, \ldots, N$ and not for the $2N$ complex unknowns D_n in (**15**). Equating the real and imaginary parts of (37) for $m = 1, 2, \ldots, N$ gives a $2N \times 2N$ real linear system to be solved for the unknown coefficients D_n. Since we use the orthogonal and conjugate properties, the linear system solved here is one-fourth the size of that for the equivalent truncation in (**15**).

4. Results

Solution of the linear system

We have found the algebraic system (37) to be rather ill-conditioned. Double-precision arithmetic is required even for modest N. Surprisingly, we find that using Gaussian elimination on the complex system does not yield results as accurate as solving the same system with twice the number of real equations. Presumably there are advantages in pivoting the real and imaginary parts separately.

As we shall show, the solutions exhibit oscillations. An attempt to inhibit these oscillations by overdetermining the system was unsuccessful; that is, taking more inner products than basis functions had little effect on the solution convergence or the oscillations.

Matching

To compare the matching procedures, we define an E_2 (or RMS) error as

$$E_2 = \left\{ \frac{1}{M} \sum_{m=1}^{M} \frac{1}{r_m} [Q_{\text{in}}(r_m) - Q_{\text{out}}(r_m)]^2 \right\}^{\frac{1}{2}}, \tag{42}$$

where Q represents a flow quantity and M is the number of evenly-spaced collocation points in the r-direction such that $r_m = m/M$. This error definition is a discretized version of the L_2-norm corresponding to the inner product weighted by $1/r$. The value of M we use is 500, which is significantly more than twice the number of oscillations in the error.

The matching of the stream function at the exit is quite good both for the method of Trogdon and Joseph (**15**) and for that presented above. Instead, we compare the axial and radial velocities, where the oscillations occur. Figures 3 show the matching of the axial and radial velocities inside and outside the die for three values of N using the adjoint method and when the surface tension and slip coefficients are zero. Note that the number of oscillations is half the truncation number N. In all cases, the inner-expansion flow variables oscillate about the outer-expansion solution, which is relatively free of oscillations. These 'Gibbs' oscillations are common at boundary-condition discontinuities. The results using the inner-product $rJ_1(q_n r)$ method from (**15**) are more sensitive to an apparent singularity at $r = 0$ (**21**).

The convergence of E_2 is shown in Fig. 4 for the adjoint method and the method of Trogdon and Joseph (**15**) for the case with zero surface tension and slip. For the adjoint method, the radial and axial velocities converge roughly as $O(N^{-\frac{1}{2}})$ and the stream function at a rate greater than $O(N^{-1})$. The spurious velocity oscillations do not decrease with increasing truncation number N for the method of Trogdon and Joseph as shown in Fig. 4. The convergence rates for both methods are unaffected by adding surface

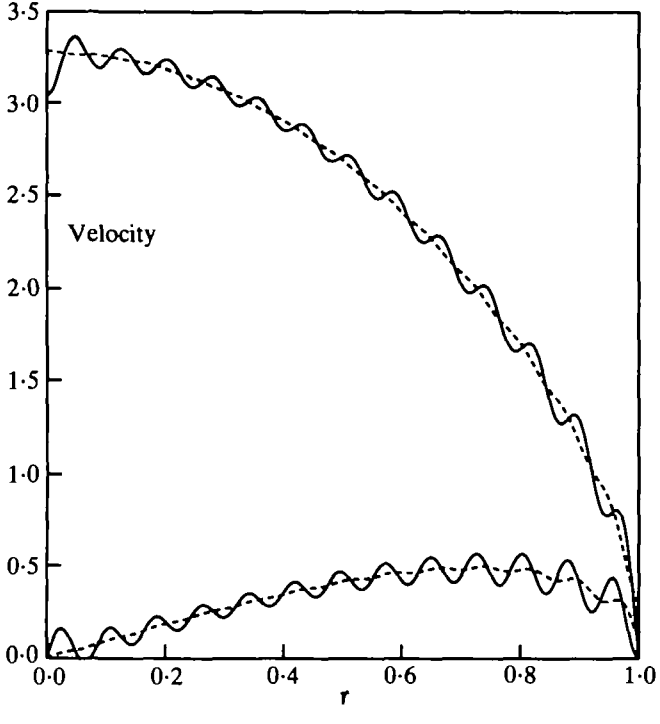

FIG. 3. Velocity matching at the exit $x = 0$: —— velocities inside the die; ····· velocities outside the die. The axial velocities, in contrast to the radial velocities, are non-zero at the centre-line $r = 0$. (a) $N = 25$

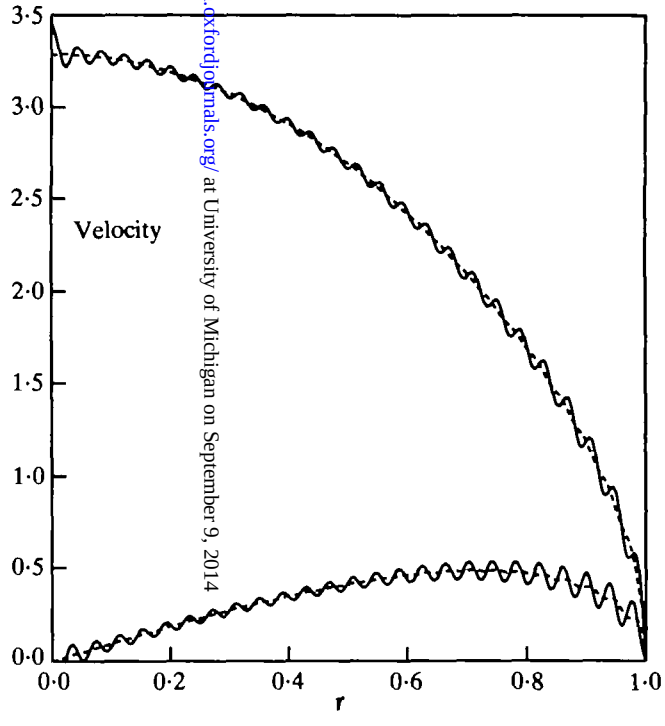

FIG. 3. (b) $N = 50$

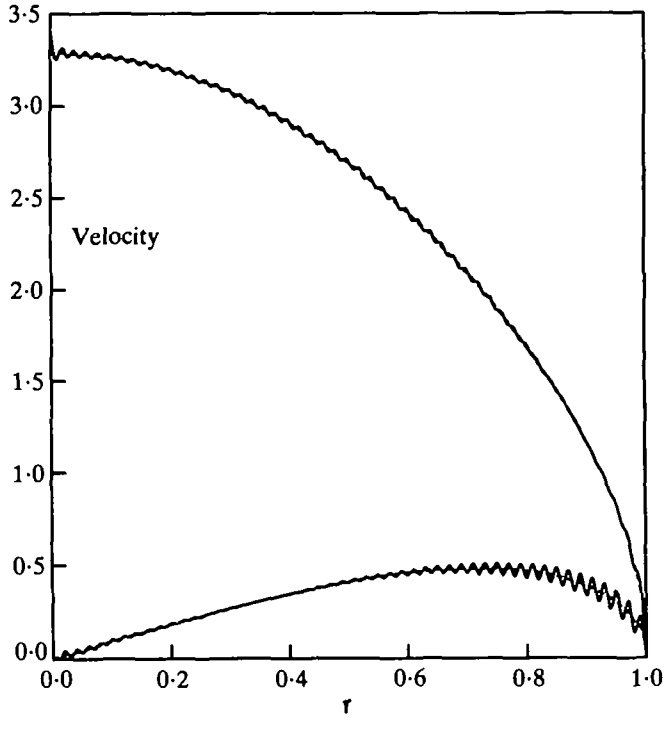

FIG. 3. (c) $N = 100$

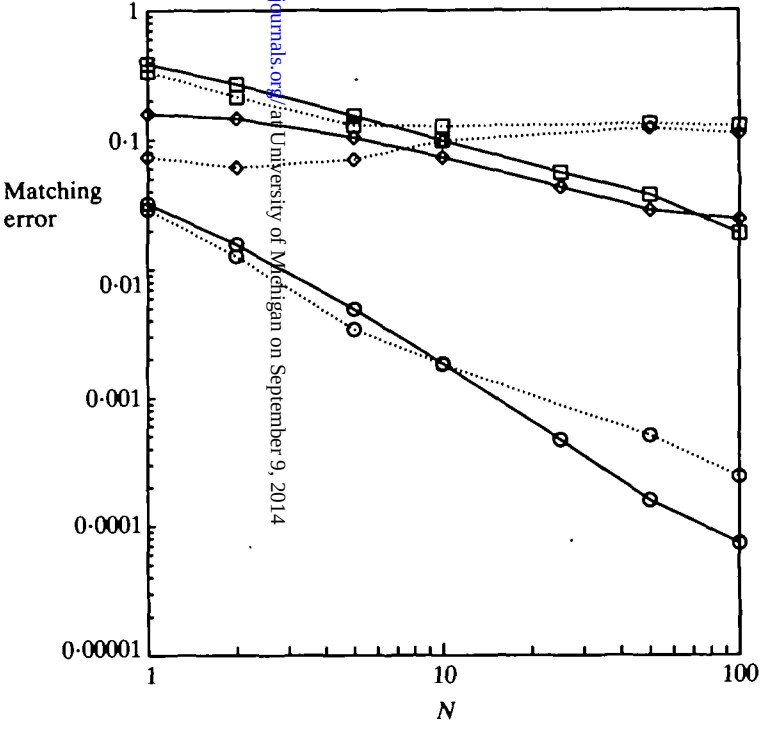

FIG. 4. RMS matching convergence: —— adjoint eigenfunction method; ····· the method of Trogdon and Joseph (**15**); ○ stream function; □ axial velocity; ◇ radial velocity

tension since the strength of the singularity is not modified. In the case of infinite surface tension, we recover the coefficients given by Trogdon and Joseph (**14**) when we use their method. Other than the poorer matching at the exit of the Trogdon and Joseph method, the two methods show similar results.

The stresses, as expected from their higher derivatives, show larger amplitude oscillations and they do not converge with increasing truncation (**21**). Because the shear stress is discontinuous at the exit, we would expect larger stress oscillations in this global approach. Presumably some convergence acceleration procedures could be applied to get the stresses to converge.

Free-surface profiles

The free-surface swell is shown in Fig. 5 for various values of $(\mathrm{Ca}\, U_f)^{-1}$. The swell is largest for zero surface tension; about 11·3 per cent. The free-surface slope η' is shown for small and zero surface tensions and different N in Fig. 6. This shows that small surface tension and truncation play an important role only near the exit. It appears that η' at the origin is converging to zero for large N (represented by a linear slope as $z \to 0$ on this log-log plot).

The convergence of $\eta'(0)$ is shown in Fig. 7 for zero and small surface tension. The curve for $\mathrm{Ca}^{-1} = 0$ is consistent with $\eta'(0) \to 0$, although at a slow algebraic convergence rate $O(N^{-\frac{1}{2}})$. The convergence is slow at the origin because the exponential decay of the eigenfunction does not contribute at $z = 0$. The most important conclusion that can be drawn from Fig. 7 is that the global analysis appears to agree with the local analysis in the limit of infinite truncation number. We find from the global analysis that the free-surface slope exiting the die is zero. Previous global analyses have not been able to satisfactorily demonstrate that local and global solutions agree.

In section 2 we indicated that the free surface is no longer constrained to separate at $\eta'(0) = 0$ when surface tension is non-zero. The curve for $\mathrm{Ca}^{-1} = 0{\cdot}1$ in Fig. 7 shows that contrary to the macroscopic view of the separation trends in Fig. 5, the separation angle can appear to increase when surface tension is added. For the limits of the truncation used, it is unclear whether $\eta(0) \to 0$ for this surface-tension value. On the other hand, it is quite clear that $\eta'(0)$ is not converging to zero for the larger surface-tension curve $\mathrm{Ca}^{-1} = 1$.

Effect of adding slip

We have indicated that increased surface tension does not improve the matching convergence, since it does not affect the singularity. Adding slip relieves the singularity, and hence, even small values of slip can improve the convergence, as shown in Fig. 8. This figure reproduces the adjoint results

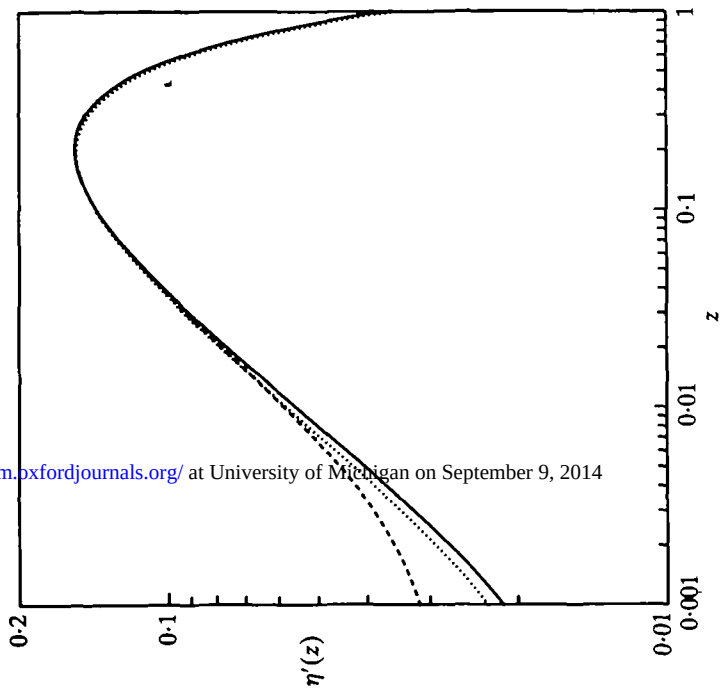

FIG. 6. Free-surface slope: —— $Ca^{-1} = 0$, $N = 400$; ..... $Ca^{-1} = 0{\cdot}1$, $N = 400$; ····· $Ca^{-1} = 0$, $N = 100$

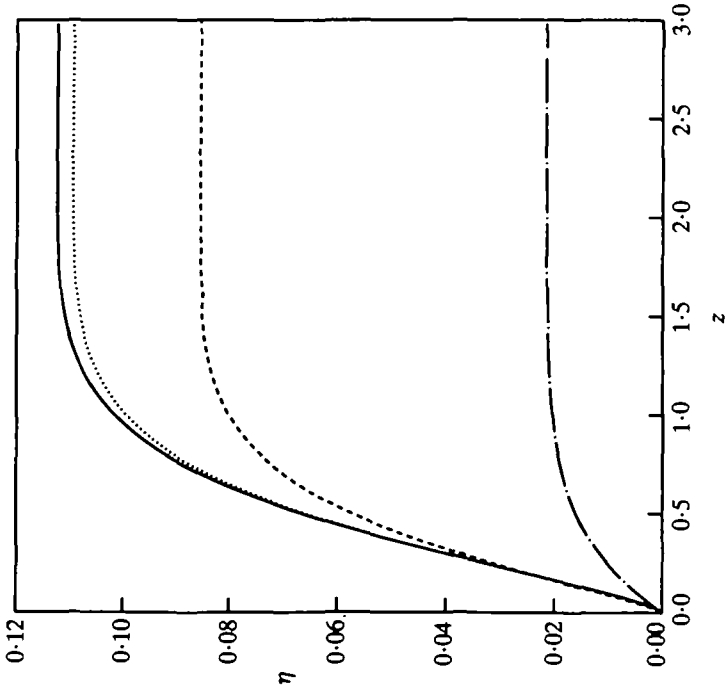

FIG. 5. Free-surface shape for varying surface tensions with $N = 200$; —— $Ca^{-1} = 0$; ..... $Ca^{-1} = 0{\cdot}1$; ····· $Ca^{-1} = 1$; —·—·— $Ca^{-1} = 10$

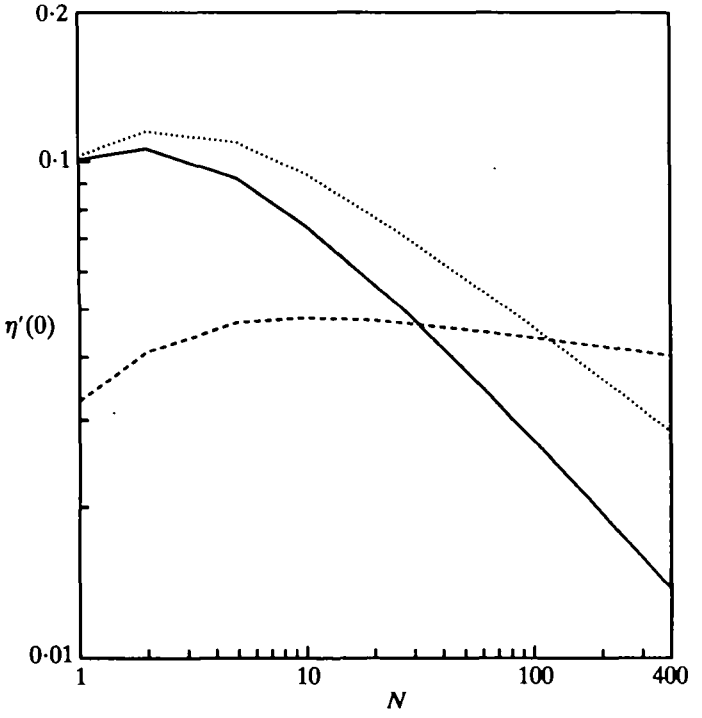

FIG. 7. Convergence of free-surface slope at exit: —— $Ca^{-1} = 0$; ····· $Ca^{-1} = 0{\cdot}1$; ····· $Ca^{-1} = 1$

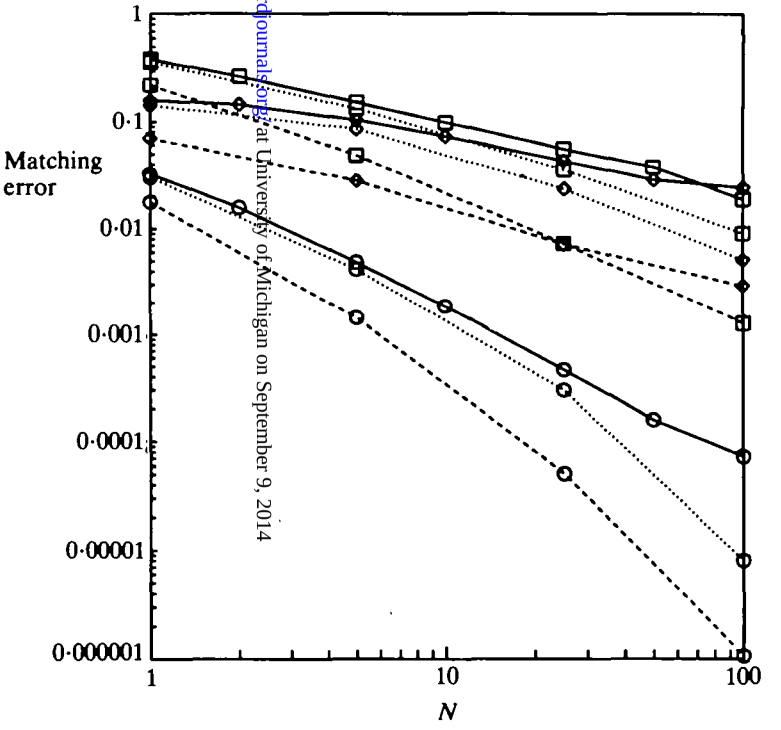

FIG. 8. RMS matching convergence with slip: —— no slip $\beta = 0$; ····· $\beta = 10^{-2}$;
○ stream function; □ axial velocity; ◇ radial velocity

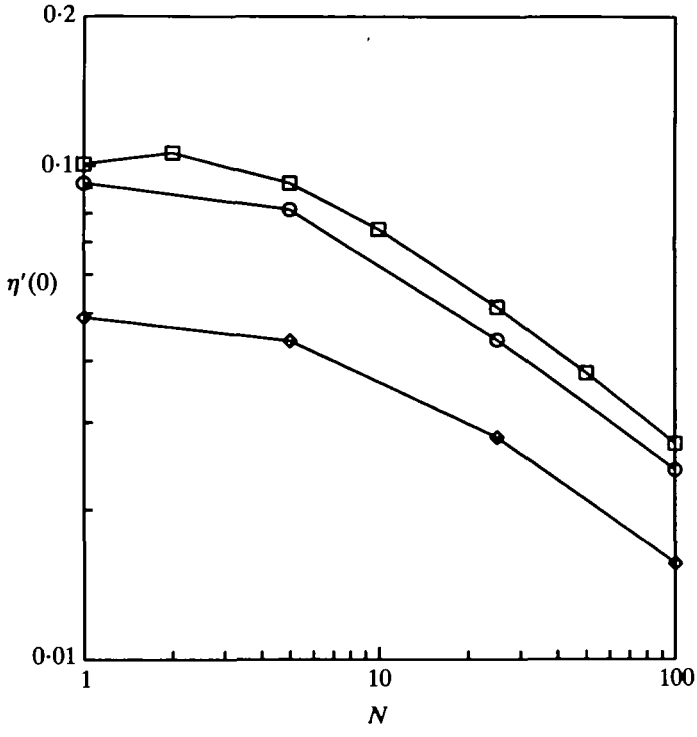

FIG. 9. Convergence of free-surface slope at exit with $Ca^{-1} = 0$: □ $\beta = 0$; ○ $\beta = 0{\cdot}01$; ◇ $\beta = 0{\cdot}1$

in Fig. 4 for zero surface tension and no slip and adds the convergence curves for the same method when small slip, $\beta = 0{\cdot}01$, is added. These figures show trends toward exponential convergence, typical of spectral results applied to problems without singularities. Adding more slip greatly improves the matching convergence.

We also indicated in section 2 that the free surface is still constrained to separate at $\eta'(0) = 0$ when slip is present. Figure 9 shows the convergence of $\eta'(0)$ when slip is added to the zero-surface-tension solution. It is easily seen that slip facilitates the convergence to $\eta'(0) \to 0$.

5. Conclusions

The global analysis presented here agrees with the local analysis presented by Michael (7). This states that the free-surface slope at the die is zero when surface tension is absent. Discrepancies between these computations and experiments or other computations can be explained by very high or infinite free-surface curvature at the exit. The solution convergence is slow at the exit; consequently, many terms are needed. Using the inner

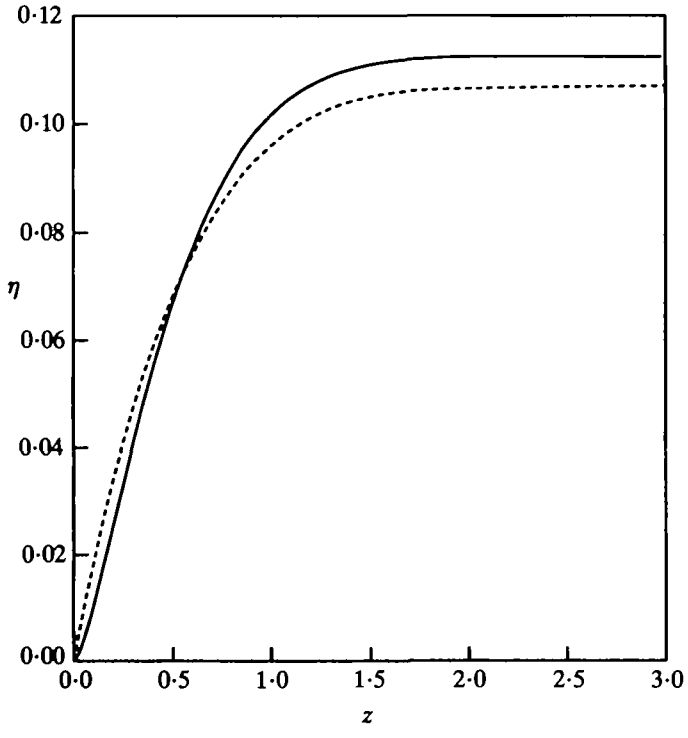

FIG. 10. Error in kinematic boundary condition from linearization: —— free-surface location from (15); ····· free-surface location where $\psi = 1$

product with the adjoint reduces the size of the linear system by half, allowing us to use more terms than the Trogdon and Joseph method for the same computation power. Perhaps more importantly, the size of the oscillations is reduced, giving closer matching and faster convergence.

There are two problems with the approach used in this study. The first is that the slow convergence requires extrapolation to infinite truncation to reach some of the conclusions. This is typical of the use of global methods on problems that have singularities (**22**). We expect that the solution convergence could be improved using acceleration techniques (a simple application of Shanks's transformation did not help), but the best approach would be to handle the singularity separately. We are presently undertaking this task using singular finite-element methods (**10**).

The second problem is that the boundary conditions are linearized about a cylindrical surface with no swell. This assumes that η and η' are small, which we can now check a posteriori. The value of η is approximately 0·1 while the largest value of η', occurring for zero surface tension, is less than 0·16, the same order as the jet swell. We can check our linearization

assumptions more carefully by testing the fully nonlinear boundary conditions. For example, we compare the location where $\psi = 1$ to the free-surface location predicted by (15) in Fig. 10. For this example, we see that the agreement is less than satisfactory, although the convergence trends of the separation angle are similar. It can be shown that adding slip or surface tension makes the linearization more appropriate.

It is obvious that a fully nonlinear approach using singular finite-element methods is desired to confirm these observations.

Acknowledgments

We wish to thank Abdel Zebib for his useful discussions and logistic support. This work was supported by National Science Foundation contracts MSM-8504456 and DMC-8716766.

REFERENCES

1. R. E. Nickell, R. I. Tanner and B. Caswell, *J. Fluid Mech.* **65** (1974) 189.
2. B. J. Omodei, *Comput. & Fluids* **8** (1980) 275.
3. P.-W. Chang, T. W. Patten and B. A. Finlayson, *Comput. & Fluids* **7** (1979) 285.
4. M. J. Crochet and R. Keunings, *J. non-Newtonian Fluid Mech.* **7** (1980) 199.
5. J. Gavis and M. Modan, *Phys. Fluids* **10** (1967) 487.
6. B. A. Whipple and C. T. Hill, *AIChE J.* **24** (1978) 664.
7. D. H. Michael, *Mathematika* **5** (1958) 82.
8. M. R. Apelian, R. C. Armstrong and R. A. Brown, *J. non-Newtonian Fluid Mech.* **27** (1988) 299.
9. W. J. Silliman and L. E. Scriven, *J. comput. Phys.* **34** (1980) 287.
10. G. Georgiou, L. G. Olson, W. W. Schultz and S. Sagan, *Int. J. num. Meth. Fluids* **9** (1989) 1353.
11. L. D. Sturges, *J. non-Newtonian Fluid Mech.* **6** (1979) 155.
12. J.-M. Vanden-Broeck, *J. Fluid Mech.* **133** (1983) 255.
13. R. I. Tanner, H. Lam and M. B. Bush, *Phys. Fluids* **28** (1985) 23.
14. S. A. Trogdon and D. D. Joseph, *Rheol. Acta* **19** (1980) 616.
15. —— and ——, *ibid.* **20** (1981) 660.
16. S. Richardson, *Proc. Camb. phil. Soc.* **67** (1970) 477.
17. L. D. Sturges, *J. non-Newtonian Fluid Mech.* **9** (1981) 357.
18. H. K. Moffatt, *J. Fluid Mech.* **18** (1964) 1.
19. R. C. T. Smith, *Austral. J. Sci. Res.* **5** (1952) 227.
20. J. Y. Yoo and D. D. Joseph, *SIAM J. appl. Math* **34** (1978) 247.
21. C. Gervasio, Masters Thesis, Rutgers University (1986).
22. W. W. Schultz, N. Y. Lee and J. P. Boyd, *J. Sci. Comput.* **4** (1989) 1.